

Relevance of electron spin dissipative processes on Dynamic Nuclear Polarization *via* Thermal Mixing

Sonia Colombo Serra¹, Marta Filibian², Pietro Carretta², Alberto Rosso³ and Fabio Tedoldi¹

¹*Centro Ricerche Bracco, Bracco Imaging Spa, via Ribes 5, 10010 Collettero Giacosa (TO), Italy.*

²*Dipartimento di Fisica and Unità CNISM, Università di Pavia, 27100 Pavia, Italy.*

³*Université Paris-Sud, CNRS, LPTMS, UMR 8626, Orsay F-91405, France.*

The available theoretical approaches aiming at describing Dynamic Nuclear spin Polarization (DNP) in solutions containing molecules of biomedical interest and paramagnetic centers are not able to model the behaviour observed upon varying the concentration of trityl radicals or the polarization enhancement caused by moderate addition of gadolinium complexes. In this manuscript, we first show experimentally that the nuclear steady state polarization reached in solutions of pyruvic acid with 15 mM trityl radicals is substantially independent from the average internuclear distance. This evidences a leading role of electron (over nuclear) spin relaxation processes in determining the ultimate performances of DNP. Accordingly, we have devised a variant of the Thermal Mixing model for inhomogeneously broadened electron resonance lines which includes a relaxation term describing the exchange of magnetic anisotropy energy of the electron spin system with the lattice. Thanks to this additional term, the dependence of the nuclear polarization on the electron concentration can be properly accounted for. Moreover, the model predicts a strong increase of the final polarization on shortening the electron spin-lattice relaxation time, providing a possible explanation for the effect of gadolinium doping.

I. INTRODUCTION

Among the different techniques which allow the nuclear spin polarization to be enhanced to almost its maximum theoretical value, Dynamic Nuclear Polarization (DNP) is raising in popularity. The method is flexible enough to be applied to a variety of molecules of biological interest that in recent years has catalyzed dramatic advances for *in vivo* ¹³C Magnetic Resonance Imaging (see the reviews [1, 2]). DNP increases the nuclear steady state polarization through a transfer of spin order between the electron and the nuclear spin systems, occurring when the Electron Spin Resonance (ESR) line is suitably irradiated. For biomedical imaging purposes this transfer takes place among the electrons of stable radicals and the nuclei of biomolecules, in a solution which is cooled to $T \simeq 1.2$ K. Once the nuclear polarization process has taken place, the frozen solution is rapidly dissolved (while maintaining most of the spin order just created [3]) and injected in living subjects to eventually image the metabolic fate of the hyperpolarized substrates *in vivo*.

In parallel to the development of these novel biomedical applications, a renewed commitment towards the understanding of the physical mechanisms driving DNP is emerging. The basic physical concepts underlying DNP phenomenology, have already been described few decades ago (see [4] and reference therein) and three different regimes, the Solid Effect, the Cross Effect and the Thermal Mixing (TM) regime, were specified according to the typical parameters of the system, such as the nuclear resonance frequency, the strength of the interaction between the spins and that of the external magnetic field. Considerable steps forward recently have been made in the quantum mechanical description of Solid Effect [5–7] and Cross Effect [8, 9]. The relevant regime for biomed-

ical application, however, has been argued to be the TM regime [10], where the electron resonance line is inhomogeneously broadened and the interactions among the spins of the electron and the nuclear system are strong.

The traditional approach to the TM regime is based on an effective thermodynamic model (the so-called spin temperature approach): such description, while providing a qualitative picture of the expected steady state polarization under microwave saturation, does not explicitly take into account the role of the concentration of the nuclear and of the radical electron spins, as well as the electron and nuclear spin relaxation rates and the electron-nucleus interactions. Improvements to the original theoretical picture have been proposed in [11] and [12, 13]. In these latter papers, in particular, a novel approach based on rate equations has been introduced, that overcomes several limits of the traditional approaches and provides a full computation of the spin dynamics. There are however certain experimental observations (see Appendix A for details) pointing out a complexity of the DNP phenomenon that remains fully unexplained. The typical DNP formulations that guarantee an adequate polarization level for *in vivo* procedures are normally obtained using relatively low concentration of trityl radicals (between 10 and 20 mM), but no exhaustive explanation of why a higher concentration of electron spins causes a reduction of the final nuclear polarization was given so far. Moreover, according the observation first reported in [10, 14], trace amounts (1-2 mM) of gadolinium complexes added to the solutions can further improve the DNP signal enhancement. The addition of gadolinium, now commonly exploited in standard protocols for DNP sample preparation [15–32], was shown to affect neither the electron linewidth nor the nuclear spin-lattice relaxation time, while it induces a reduction of the electron

spin relaxation time T_{1e} [10, 33] which, nevertheless, is by far too small to account for the positive effect on nuclear polarization in the framework of the available theoretical descriptions [10].

In this paper we first integrate the available experimental scenario with new data, collected on a prototype trityl doped sample (Section II), showing how the final value of the nuclear polarization does not depend on the concentration of nuclear spins. Inspired by such observation, in Section III we introduce a variant of the rate equation approach proposed in [12], which includes a dissipative term within the electron system controlled by the radical concentration. The numerical predictions of this novel model, reported in Section IV, reproduce rather well the experimental behaviour of the nuclear polarization *versus* electron spin density as well as its extreme sensitivity to the reduction of T_{1e} . These and other aspects of the comparison between theoretical and experimental results (these latter recalled in Appendix A) are discussed in more detail in Section V. All technical details of the model computation have been included in Appendix B, to better highlight the main messages of this work.

II. DEPENDENCE OF STEADY STATE POLARIZATION ON NUCLEAR CONCENTRATION

The steady state nuclear polarization $P_n^\infty = P_n(t \rightarrow \infty)$ predicted by the theoretical models available so far, under the assumption that the only energy exchange between the spin systems and the lattice occurs *via* T_{1e} , are usually overestimated. Thus the TM theory should properly take into account also other dissipative mechanisms. In order to clarify whether these mechanisms involve primarily the electron or the nuclear spin reservoir, we have

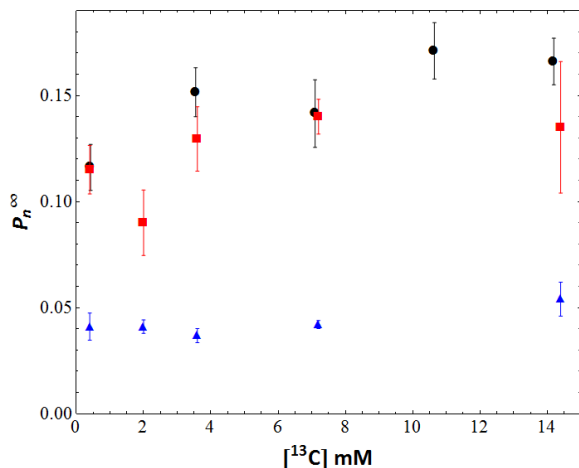


FIG. 1: Optimal P_n^∞ as a function of the [$1\text{-}^{13}\text{C}$] labelling rate for a sample of pyruvic acid doped with OX063 trityl radical 15 mM measured at $B \approx 3.35$ T and at a temperature in the range 1.2 – 4.2 K.

experimentally investigated the modifications of P_n^∞ in pyruvic acid samples doped with OX063 trityl radical 15 mM at variable ^{13}C concentration.

To keep all the other properties of the solution unchanged, samples with different ^{13}C concentrations were obtained by mixing unlabelled pyruvic acid and [$1\text{-}^{13}\text{C}$]-pyruvic acid in different ratios. The carbon nuclear system of the unlabelled product is made by $\approx 99\%$ spinless ^{12}C , whereas in fully labelled [$1\text{-}^{13}\text{C}$]-pyruvic acid, 1/3 of the carbon nuclei have spin $S = 1/2$, since each pyruvic molecule has 3 carbons but only those in position-1 are ^{13}C enriched.

^{13}C polarization measurements were performed using two different apparatus operating at about the same magnetic field B but with different capabilities of temperature-regulation, to check whether or not the information we look for is temperature dependent. The first DNP system operates at $B = 3.35$ Tesla at 1.2 K and is equipped with a 0-200 mW microwave source that can be swept between 93.75 and 94.25 GHz and with a 35.86 MHz Radiofrequency (RF) set up. The second one works at variable temperature in the 1.8-4.2 K range and uses a 32 mW Gunn Diode MW Source working in the range 95.96-98.04 GHz and a 37.05 MHz RF probe. All the samples underwent flash freezing in a cryogenic bath prior to starting MW irradiation. The ^{13}C NMR signal build up was sampled after RF saturation by means of low flip angle (α about 6°) acquisitions [3]. P_n^∞ and the polarization time T_{pol} were derived by fitting the build up curves to an expression that properly takes into account the reduction of the ^{13}C signal amplitude with time induced by the readout pulses.

For low ^{13}C concentrations the evolution of the nuclear polarization turned out to be very slow (at 1.2 K $T_{\text{pol}} \approx 4000$ s for the sample at natural abundance *vs* ≈ 1000 s for the fully labelled sample), reflecting a degradation of the electron-nucleus contact on increasing the average distance between the two spin species and a slow nuclear spin diffusion. However, at all the investigated temperatures the final value of P_n^∞ was found to be nearly independent from the ^{13}C concentration [^{13}C] (FIG. 1), similarly to what reported also for other samples polarized by means of nitroxides radicals [34]. This suggests that P_n^∞ is substantially unaffected by nuclear relaxation mechanisms that do not involve the electron reservoir. In fact, as remarked in [13], in presence of a sizeable direct exchange between the nuclear system and the lattice, one would expect a substantial decrease of P_n^∞ on decreasing the electron-nucleus contact. Thus, it is concluded that the reduction of P_n^∞ should primarily originate from dissipative processes involving the electron spins.

III. THEORETICAL MODEL

The TM regime is characterized by a large spread of electron Larmor frequencies (much larger than the nu-

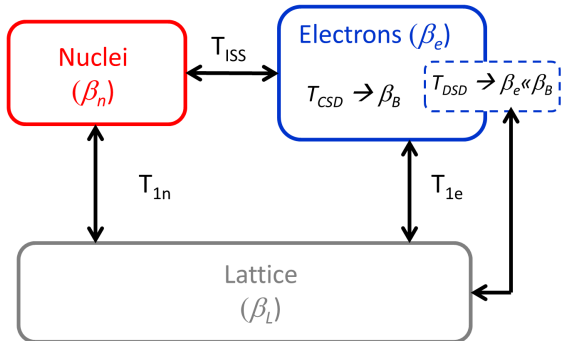


FIG. 2: Thermal systems and interactions involved in TM-DNP. Nuclei directly feel the lattice through the leakage term T_{1n} which represents the nuclear relaxation processes not mediated by electrons. *Via* the three particle mechanism T_{ISS} electrons are in contact with the nuclear system, while thermalizing internally by energy conserving spectral diffusion (T_{CSDD}) and with the lattice by Zeeman transitions (T_{1e}). Moreover, in the model presented here, electron spins also interact among themselves and with the lattice through dissipative spectral diffusion (T_{DSD}).

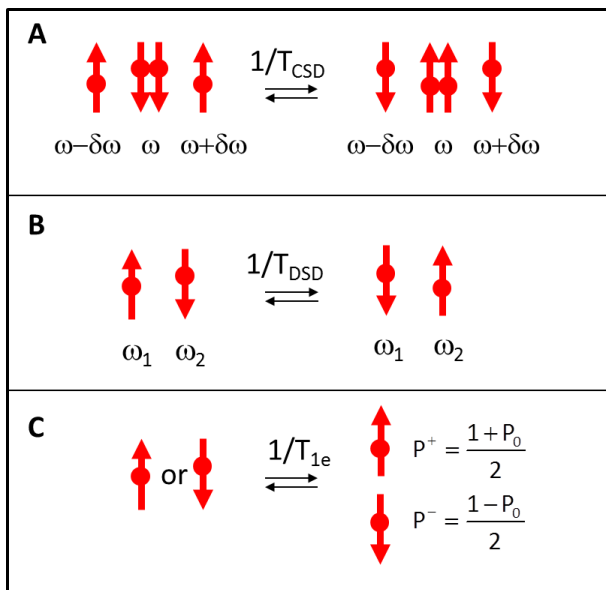


FIG. 3: Microscopic interactions driving the evolution of the electron polarization profile under the assumption of bad contact between electrons and nuclei and negligible leakage ($T_{ISS}, T_{1n} \rightarrow \infty$). A: energy conserving spectral diffusion. B: dissipative spectral diffusion (electron electron flip-flop). C: electron spin-lattice relaxation towards the Boltzmann equilibrium polarization $P_0 = -\tanh[\beta_L \omega_e]$.

clear Larmor frequency ω_n), arising from a distribution of local magnetic fields as, for example, in presence of a g -tensor anisotropy. In these conditions it is useful to

split the electron population into spin packets sharing the same Larmor frequency. The convolution of these packets yields the ESR line. At a given frequency ω the intensity of the ESR line $f(\omega)$ is proportional to the number of electrons resonating at that frequency. The function $f(\omega)$ and the average electron frequency ω_e are defined so that $\int f(\omega) d\omega = 1$ and $\int (\omega - \omega_e) f(\omega) d\omega = 0$. In a magnetic field strength of the order of 1 T, at a temperature T_L of 1 K, the electron system is highly polarized and assumes a nearly constant profile:

$$P_e^0(\omega) \approx P_e^0(\omega_e) = P_0 = \tanh[\beta_L \omega_e] \quad (1)$$

where $\beta_L = \hbar / (2k_B T_L)$, with \hbar and k_B indicating the reduced Planck constant and the Boltzmann constant respectively, is the inverse lattice temperature (notice that, as here, it is normally reported in time units).

Under microwave irradiation the electron spin system moves from Boltzmann equilibrium to a non-equilibrium steady state, characterized by a frequency-dependent profile $P_e^\infty(\omega)$ which is responsible for the enhancement of the nuclear polarization. In order to describe this phenomenon it is convenient to consider the three different subsystems sketched in FIG. 2:

- the lattice, which is insensitive to microwave (MW) irradiation and is characterized by a constant inverse temperature β_L ;
- the electron spin system which is forced by MW towards a non uniform steady state profile $P_e^\infty(\omega)$ that, according to the spin temperature approach, corresponds to an inverse temperature β_e much higher than β_L ;
- the nuclear spin system characterized by an inverse temperature β_n , so that $P_n^\infty = \tanh(\beta_n \omega_n)$.

In general, the computation of β_e is a rather difficult task since the electron spins, which are strongly interacting with each other *via* dipolar coupling, are out of equilibrium due to MW irradiation and are at the same time in contact with a thermal bath (lattice). Under certain assumptions, discussed in detail below, Borghini [4, 35] was able to compute $P_e^\infty(\omega)$ and, accordingly, its corresponding inverse temperature $\beta_e = \beta_B$, and to provide an upper bound for P_n^∞ . His overestimation is particularly evident when MW irradiation is performed at the edges of the ESR line where one would expect to observe an almost negligible polarization enhancement, while rather sizeable values are predicted by the Borghini's model. In previous works [12, 13] we showed that a finite electron nucleus contact, even in the mean field approximation, allows to recover realistic values of the nuclear spin polarization. In that model the finite electron-nucleus contact combines both the ISS processes (a simultaneous flip-flop of two electron spins compensated by a nuclear spin flip) and the nuclear spin diffusion. Nuclei reach an intermediate inverse spin temperature between β_L and β_B , corresponding to a reduced P_n^∞ , and determined by the

ratio between the electron-nucleus contact (quantified by T_{ISS}) and the nuclear leakage (T_{1n}). By properly tuning the values of these parameters, one reproduces MW spectra similar to those observed in experiments. However, according to such a model one would expect T_{ISS} to increase both with the nuclear and with the electron spin concentration that, by improving the contact among the two spin systems, would reduce the relative efficiency of the leakage, leading to higher steady state polarization levels. Since this does not correspond to the behaviour observed experimentally (see also Section II), it becomes necessary to go beyond the profile $P_e^\infty(\omega)$ proposed by Borghini and search for different electron steady states, characterized by an inverse temperature β_e smaller than β_B and dependent on the electron spin density.

First of all, it has to be realized that the Borghini model and the model introduced in [12, 13] rely on the assumption that the energy exchange between the electron system and the lattice occurs only *via* the Zeeman transitions depicted in FIG. 3, panel C, whereas all transitions involving more than one electron spin are always energy conserving. The simplest microscopic process of this kind, characterized by a time-scale T_{CSD} [44], is depicted in FIG. 3, panel A. Transitions involving more than one spin are the elementary events of the phenomenon referred to as spectral diffusion in the low temperature TM-DNP description proposed in [4]. Here we will call it *energy conserving* spectral diffusion (CSD) for the reasons that will become clear at the next paragraph. When CSD is infinitely efficient ($T_{CSD} = 0$), the electron system is driven towards a high inverse temperature β_B .

In this manuscript we consider an alternative model based on three main realistic assumptions. *First*, the energy conserving spectral diffusion is not, as it was always assumed so far in the TM models, infinitely fast ($T_{CSD} \neq 0$). *Second*, non conserving electron flip-flop processes (characterized by a time constant T_{DSD}) are possible. The most elementary non conserving transition is represented in FIG. 3, panel B. These latter events, analogously to T_{CSD} processes, promote an internal thermalization among the different spin packets of the ESR line and for this reason we refer to their macroscopic effect as *dissipative* spectral diffusion (DSD). Since at $T \approx 1$ K, the typical temperature where the most remarkable enhancements are obtained, the lattice bath is almost fully frozen, we expect T_{DSD} to be much longer than T_{CSD} . The *third* assumption originates from the experimental results reported in the previous section, which clearly show that when trityls are exploited as polarizing agents for ^{13}C nuclei, the electron-nucleus contact $1/T_{ISS}$ and the nuclear leakage $1/T_{1n}$ are always weak enough to make any electron polarization loss *via* the nuclear channel irrelevant in defining the final steady state of electrons. In this limit $P_e^\infty(\omega)$ is determined only by the competition between energy conserving and non conserving processes and can be derived, upon considering the electron spins as a fully connected system, by solv-

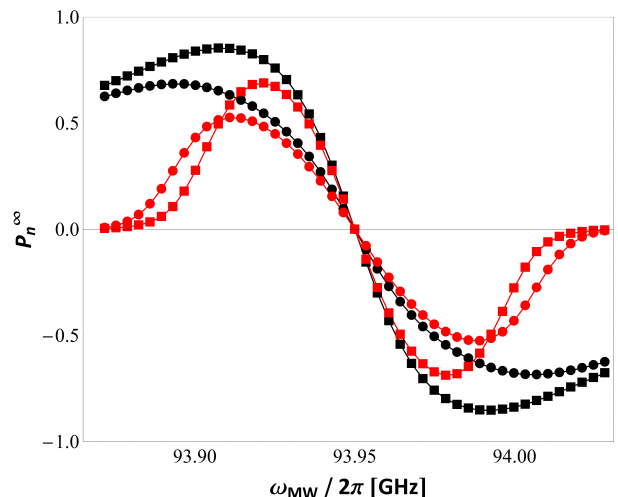


FIG. 4: P_n^∞ MW spectra on varying T_{CSD} and T_{DSD} . Black squares: Borghini model. Red squares: behaviour obtained from Eq.s 2 and B1 with $T_{1e} = 1$ s, $T_{CSD} = 10^{-7}$ s and $1/T_{DSD} = 0$. Black circles: from Eq.s 2 and B1 with $T_{1e} = 1$ s, $T_{CSD} = 0$ s and $T_{DSD} = 10^{-3}$ s. Red circles: from Eq.s 2 and B1 with $T_{1e} = 1$ s, $T_{CSD} = 10^7$ s and $T_{DSD} = 10^{-3}$ s.

ing a system of mean field rate equations (Appendix B) describing the three processes in FIG. 3. Once $P_e^\infty(\omega)$ is known, the corresponding nuclear polarization P_n^∞ is derived as described in [13] (see Eq.(9)) through the following equation:

$$P_n^\infty = \frac{\int f(\omega)f(\omega + \omega_n) [P_e^\infty(\omega) - P_e^\infty(\omega + \omega_n)] d\omega}{\int f(\omega)f(\omega + \omega_n) [1 - P_e^\infty(\omega)P_e^\infty(\omega + \omega_n)] d\omega}. \quad (2)$$

IV. NUMERICAL RESULTS

Numerical simulations have been performed implementing the rate equation system (B1) for the electron profile and the equation (2) for the nuclear polarization. The external magnetic field is set to $B_0 = 3.35$ T and the temperature to 1.2 K in agreement with most of the experimental measurement conditions. To model the ESR line of trityl radicals, we have chosen a Gaussian shape centered at $\omega_0 = 2\pi$ 93.95 GHz, according to [33] (further details in Appendix B). Let us first look at the effect of a finite $1/T_{CSD}$ rate and of a non vanishing dissipative spectral diffusion $1/T_{DSD}$ on the steady state nuclear polarization. In FIG. 4 the P_n^∞ as a function of the MW irradiation frequency (MW spectrum) is obtained under Borghini's assumptions in absence of nuclear leakage ($T_{CSD} = 0$, $T_{ISS} = 0$ and $1/T_{1n} = 1/T_{DSD} = 0$, black squares) is plotted together with the output of our computation for the following choices of parameters:

- $T_{1e} = 1$ s, $T_{CSD} = 10^{-7}$ s and $1/T_{DSD} = 0$, red

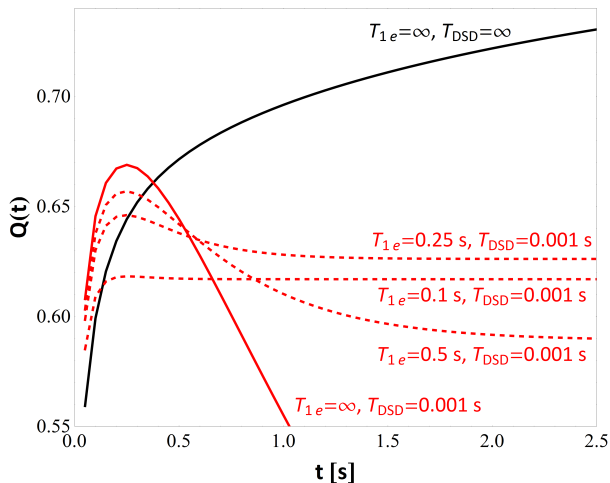


FIG. 5: Time evolution of the electron profile encoded in the scalar variable $Q(t)$ computed according to Eq.(3) upon saturating the most effective packet and setting $T_{\text{CSD}} = 10^{-7}$ s.

squares;

- $T_{1e} = 1$ s, $T_{\text{CSD}} = 0$ s and $T_{\text{DSD}} = 10^{-3}$ s, black circles;
- $T_{1e} = 1$ s, $T_{\text{CSD}} = 10^{-7}$ s and $T_{\text{DSD}} = 10^{-3}$ s, red circles.

One immediately recognizes that the assumption of a non zero, although very small, value of T_{CSD} leads to a clipping of the wings of the nuclear polarization spectrum and thus to the solution of the most evident limitation of the Borghini model that was encountered also in the high temperature TM limit first discussed by Provotorov [36–39]. A similar improvement is achievable also by assuming a combination of bad electron-nucleus contact and finite nuclear leakage [13] or by imposing a partial saturation of the irradiated packet [11, 13]. Here however it comes for free, by simply removing the non physical condition $T_{\text{CSD}} = 0$, which is more or less implicitly accepted in all TM models. As expected, the second new element of the proposed model (electron electron flip-flop), acts as a source of dissipation within the electron system, producing an overall suppression of the final nuclear polarization. Also in this case a $T_{\text{CSD}} \neq 0$ is mandatory to obtain a sharper and realistic shape of the P_n^∞ spectrum.

In order to analyze the time evolution of the electron profile $P_e(\omega, t)$, as obtained by the system of rate equations (B1), it is convenient to introduce a scalar parameter $Q(t)$ computed from $P_e(\omega, t)$ through the following equation:

$$Q(t) = \frac{\int f(\omega)f(\omega + \omega_n) [P_e(\omega, t) - P_e(\omega + \omega_n, t)] d\omega}{\int f(\omega)f(\omega + \omega_n) [1 - P_e(\omega, t)P_e(\omega + \omega_n, t)] d\omega}. \quad (3)$$

$Q(t)$ represents the nuclear polarization associated to the electron profile $P_e(\omega, t)$ frozen at the time t of its evolution toward the steady state. Let us stress that $Q(t)$ and $P_n(t)$ have rather different build up times, being the latter dependent on T_{ISS} , and converge to the same value only for $t \rightarrow \infty$.

When $T_{\text{DSD}} \rightarrow \infty$ the electron profile under MW irradiation at frequency ω_{MW} progresses from hole burning (where the irradiated packet is saturated and all other packets are at Boltzman equilibrium) to a profile which approaches, in the limit $T_{\text{CSD}} \ll T_{1e}$, the one predicted by Borghini ($P_e(\omega) = \tanh[\beta_B(\omega - \omega_{\text{MW}})]$). In the example depicted in FIG. 5 in particular, the system is shown to evolve from $Q(t = 0) = 0.34$ to $Q(t \rightarrow \infty) = 0.825$. When T_{DSD} is finite and the electron spin-lattice relaxation is negligible ($T_{1e} \rightarrow \infty$), the system starts to evolve from the hole burning profile ($Q(t = 0) = 0.34$) to larger Q values up to $t \approx T_{\text{DSD}}$, when the dissipative process becomes relevant and the saturation of the burned spin packet slowly spreads throughout the ESR spectrum ($Q(t = \infty) = 0$). This catastrophic fate is prevented by the onset of electron spin lattice relaxation which freezes the electron profile for $t > T_{1e}$. In summary two time-regimes can be identified:

- $t \ll T_{\text{DSD}}$, where CSD processes dominate and increase the nuclear polarization;
- $t \gg T_{\text{DSD}}$, where DSD processes are effective and reduce P_n^∞ .

Both the reduction of P_n^∞ observed when increasing the radical concentration and the polarization enhancement following gadolinium doping find a natural explanation within this general framework. By shortening T_{DSD} and T_{CSD} without significantly affecting T_{1e} , a larger number of paramagnetic centers depresses the nuclear polarization. On the other hand, any perturbation that solely reduces T_{1e} leaving the spectral diffusion parameters unchanged (as gadolinium doping is expected to do), has a positive outcome on P_n^∞ .

A. Effect of electron concentration

An increase of the electron concentration c leads to an enhancement of the transition rates $1/T_{\text{CSD}}$ and $1/T_{\text{DSD}}$ that depend on the mutual distances between electrons. In our simulations the two parameters were phenomenologically assumed to scale with c^2 . Beside allowing to nicely reproducing the observed experimental behavior, this choice for $1/T_{\text{DSD}}$ was suggested by the c^2 dependence reported by Abragam and Goldman in reference [4], Eq. (6.50), for the $1/T_{\text{ISS}}$ process. That process, involving the flip-flop of two electron spins with energy exchange with the nuclear reservoir is analogous to DSD process where, on the other hand energy is exchanged with the lattice. The same scaling was assumed for the CSD process which however does not lead to significant changes in the results as far as $T_{\text{CSD}} < T_{\text{DSD}}$.

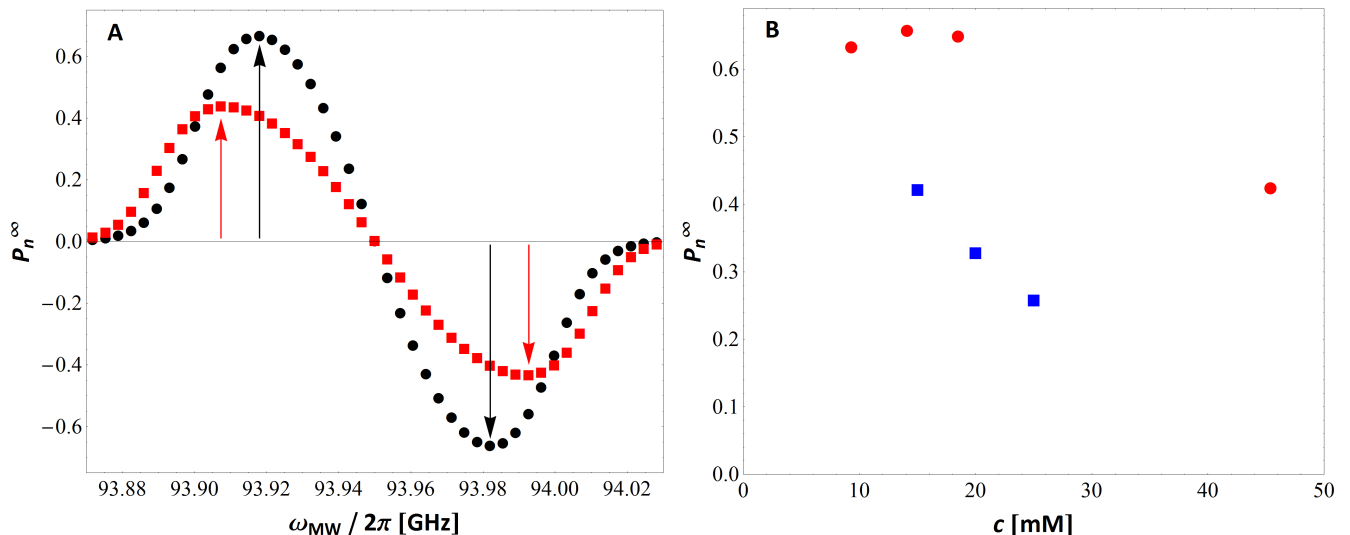


FIG. 6: Effect of electron concentration. Simulated data for systems with $T_{1e} = 1$ s. Panel A, black circles: MW spectrum obtained by setting $T_{\text{CSD}} = 10^{-7}$ s and $T_{\text{DSD}} = 5 \cdot 10^{-3}$ s, and reproducing the behaviour of a $[1\text{-}^{13}\text{C}]$ -pyruvic acid sample with trityl 15 mM. Panel A, red squares: MW spectrum obtained by scaling T_{CSD} and T_{DSD} with the electron spin concentration as specified in the text, reproducing the behaviour of a $[1\text{-}^{13}\text{C}]$ -pyruvic acid sample with trityl 45 mM. Panel B: Maximum P_n^∞ as a function of the electron spin concentration c obtained by scaling as described in the text the T_{CSD} and T_{DSD} values fitted to the $[1\text{-}^{13}\text{C}]$ -pyruvic acid sample with trityl 15 mM (red circles). The blue squares represent the behaviour obtained by setting $T_{\text{CSD}} = 10^{-7}$ s, $T_{\text{DSD}} = 5 \cdot 10^{-4}$ s to match the experimental polarization of a $[^{13}\text{C}]$ -urea sample with trityl 15 mM, and by scaling them with concentration as above. The simulated trends reflect the corresponding experimental behaviours reported in the insets of FIG. 8.

Numerical results, obtained by setting $T_{1e} = 1$ s according to [10, 33] and by adapting T_{CSD} and T_{DSD} to fit the experimental value P_n^∞ of given samples at 15 mM trityl concentration, are shown in FIG. 6, in order to properly describe the experimental behaviour found in $[1\text{-}^{13}\text{C}]$ -pyruvic acid and $[^{13}\text{C}]$ -urea samples described in Appendix A, FIG. 8. The decrease of P_n^∞ observed at high radical concentration for both systems (FIG. 6, panel B) is due to the higher efficiency of DSD processes in the regime where they are predominant. Conversely, the small increase observed for the $[1\text{-}^{13}\text{C}]$ -pyruvic acid sample at low radical concentration corresponds to the regime where CSD dominates. At very low concentration the polarization shows the correct qualitative behaviour although it can be a bit overestimated. A possible explanation is that in our approach we assume for the limit of vanishing electron concentration an hole burning shape which corresponds to a pretty high value of P_n^∞ . This assumption is quite crude because the hole burning shape is not realistic even if the electron packets are not interacting (Bloch equations).

Finally, when the whole MW spectra at two different radical concentration are considered (FIG. 6, panel A), a shift of the maximum enhancement position towards the edge of the spectra, when increasing c , is observed. To our knowledge this effect has not been assessed experimentally in detail and remains a prediction of the model.

B. Effect of gadolinium doping

The effect of doping the DNP samples with moderate quantities of gadolinium complexes has been modeled by considering the T_{1e} reduction that, according to literature data [33], follows such doping. For numerical simulations a strong (although finite) CSD diffusion has been set ($T_{\text{CSD}} = 10^{-7}$ s), whereas the spin lattice relaxation was taken from literature [10, 33] ($T_{1e} = 1$ s in absence of gadolinium). T_{CSD} was adapted in order to suitably reproducing P_n^∞ MW spectra without gadolinium. The two major effects of reducing T_{1e} are shown in FIG. 7, panel A: (i) the overall nuclear polarization is enhanced; (ii) the peaks position is shifted towards the centre of the spectrum. It should be stressed that the quantitative agreement between the simulated MW spectra and their experimental counterpart reproduced in FIG. 9 (in particular the 4-fold enhancement) is remarkable. The behaviour of the maximum P_n^∞ as a function of $1/T_{1e}$ is represented in panel B. Two regimes can be recognized: for low gadolinium concentration the nuclear polarization is enhanced since the T_{1e} reduction corresponds to a suppression of the dissipative effect induced by T_{DSD} processes; for higher gadolinium concentration P_n^∞ decreases and slowly reaches the value correspondent to the hole burning profile.

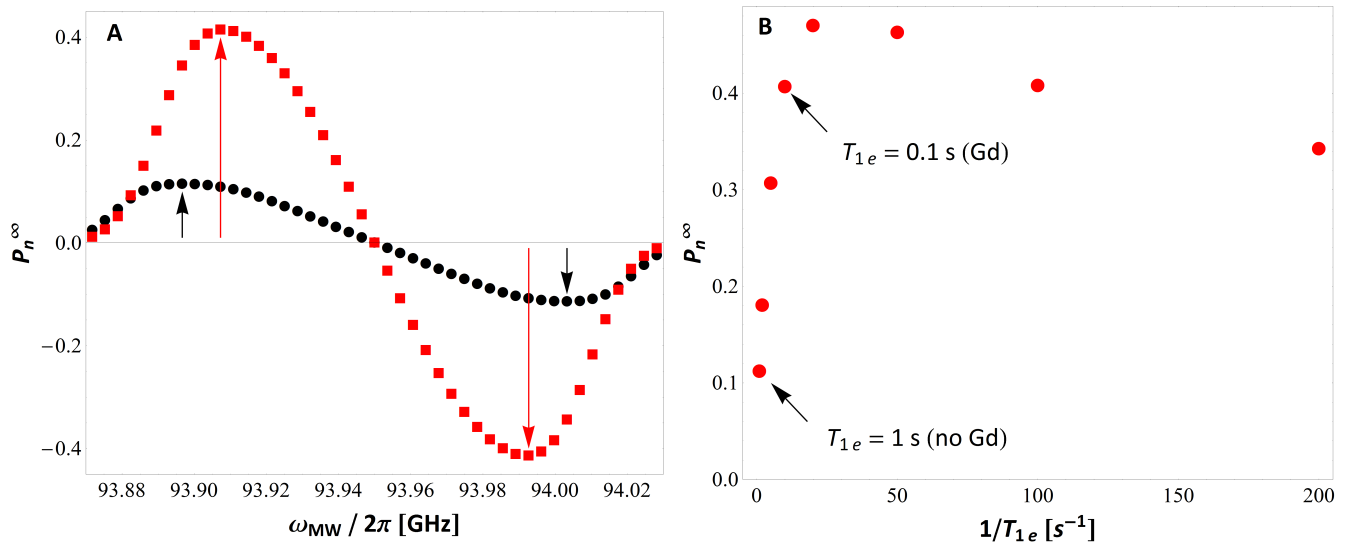


FIG. 7: Effect of gadolinium doping. Simulated data for a system characterized by the following parameters: $T_{\text{CSD}} = 10^{-7}$ s, $T_{\text{CSD}} = 5 \cdot 10^{-5}$ s. Panel A: Microwave DNP spectra upon setting $T_{1e} = 1$ s (corresponding to a sample without gadolinium, black circles) and $T_{1e} = 0.1$ s (corresponding to a sample with 1.5 mM of gadolinium, red squares). The up and down arrows indicate the approximate positions of maximum (positive and negative respectively) polarization. Panel B. Maximum P_n^∞ as a function of the electron relaxation rate T_{1e} , ranging from 5 ms to 1 s (corresponding to different gadolinium concentration).

V. DISCUSSION AND CONCLUSION

The aim of this work was to find a suitable theoretical justification for the effects of radical concentration and gadolinium doping on the ultimate performances of a DNP procedure carried out at $T \approx 1$ K with trityl radicals. The available experimental data show that P_n^∞ decreases at high trityl concentration and increases after addition of moderate amounts of gadolinium complexes. The P_n^∞ reduction on increasing the number of paramagnetic centers is associated with a faster polarization build up. While a speed up of the DNP process with the increase in the radical concentration has to be expected, since there are more polarization transfer centers, the significant decrease of the steady state polarization has not been accounted for by any previous theoretical description. In fact both the Borghini [35] and the finite contact model introduced in [12] and [13] predict no effect of the radical concentration as long as T_{1n} is negligible whereas, in presence of leakage, a higher number of polarizing centres would push the system towards higher steady state polarizations. Gadolinium doping on the other hand leaves substantially unaffected the nuclear polarization time, while shortening the typical electron spin lattice relaxation time T_{1e} . In the Borghini's framework such a reduction is expected to induce an enhancement of P_n^∞ , that however, as already remarked in [10], cannot justify quantitatively those sizeable enhancements reported in the same paper and later on in [33, 43]. To complete the experimental picture we measured the

dependence of P_n^∞ on nuclear concentration by varying the labelling percentage on a $[1-^{13}\text{C}]$ -pyruvic acid sample added with trityl radicals 15 mM. Even if at low nuclear concentration the polarization time becomes very long, the final value of P_n remains almost constant.

The main messages emerging from this collection of literature and experimental observations can be summarized as follows.

- The nuclear spin system does not affect the evolution of the electron profile, acting only as a passive viewer of the electron system.
- The transition rate of many particle processes (involving nuclear and electron spins) increases with the radical concentration.
- The addition of gadolinium complexes to the DNP preparation leads to a reduction of electron spin-lattice relaxation and to an enhancement of the steady state nuclear polarization.

Guided by these three items we introduced a novel model, based on the same rate equations approach proposed in [12] under the assumption of bad electron-nucleus contact and negligible nuclear leakage, but including an additional mechanism accounting for energy exchanges between couples of electron spins (that flip simultaneously) and the lattice. It is worth to mention that similar flip-flop processes were already introduced by Farrar *et al.* [40] in a high temperature approximation of TM-DNP in presence of inhomogeneously broadened ESR

lines. Here we implement them within a theoretical picture where conservative spectral diffusion terms are also active and no linearization of the electron and nuclear polarization has been applied. When both the conservative and non-conservative flip-flop rates $1/T_{\text{CSD}}$ and $1/T_{\text{DSD}}$ are phenomenologically assumed to scale with c^2 , our model is able to reproduce fairly well the experimental behaviour of P_n^∞ on increasing the density of paramagnetic centers (see FIG. 6 *versus* FIG. 8). A quantum mechanical derivation of the two rates, and in turn of their c -dependence, would be desirable and certainly deserve additional future work to provide a more rigorous treatment. However, it has been checked that even if other (positive) c -dependences of the flip-flop rates are assumed, the qualitative outcome of this analysis remains unchanged, although the agreement between experimental and simulated data get worse.

The implementation of the DSD, makes the model also much more sensitive to $1/T_{1e}$ variations, providing a suitable key of interpretation for the influence of gadolinium doping on nuclear polarization enhancement (see FIG. 7 *versus* FIG. 9). Remarkably the role of dissipative processes on the electron magnetic behaviour of gadolinium-doped DNP samples was anticipated by Lumata et al. [43]. Here we went over some of the assumptions limiting the theoretical analysis of the cited authors. In particular we avoided the use of the Provotorov approximation, which displays an unphysical overestimation of P_n at the edges of the MW spectrum, and we extended our investigation beyond the regime dominated by dissipative processes, where the final nuclear polarization depends monotonically on gadolinium concentration, definitely resulting in a more extensive description of the experimental scenario.

In conclusion here we have presented a theoretical model providing a broad and unified understanding of different features observed in low temperature ^{13}C DNP experiments based on the use of trityls (or narrow linewidth radicals as polarizing agents). The validity of the model is limited to those cases where the radical concentration is high enough for TM to dominate over other polarization mechanisms such as the Solid Effect, and to make the polarization build up time fast with respect to nuclear leakage processes. Moreover the model is not expected to suitably describe systems characterized by broad ESR lines, where also protons are involved in the TM mechanism (as in nitroxides). In that case (that will be object of future studies) the electron-nucleus contact and the nuclear leakage are likely to be strong enough to be involved in the evolution of the electron profile.

VI. ACKNOWLEDGEMENT

We gratefully acknowledge L. Lumata, M.E. Merritt, C.R. Malloy, A.D. Sherry and Z. Kovacs for kindly letting us reproduce their experimental data, A. De Luca for the fruitful discussion, M. Moscardini for his techni-

cal support and Albeda Research for the preparation of the sample used in the experiments described in Section II and for the stimulating exchange of views. This study has been supported in part by Regione Piemonte (Misura II.3 del Piano Straordinario per l'Occupazione), by the COST Action TD1103 (European Network for Hyperpolarization Physics and Methodology in NMR and MRI) and by the ANR grant 09-BLAN-0097-02.

Appendix A: Review of literature experimental data

The scientific literature reporting dedicated experimental studies aimed at investigating and understanding the dependence of P_n^∞ on trityl radical concentration and gadolinium doping is here briefly reviewed.

Different P_n^∞ values have been observed depending on the chemical-physical properties of the investigated sample and on the type of radical used as polarizing agent. Two compounds in particular have deserved extensive experimental studies:

- $[1-^{13}\text{C}]$ -pyruvic acid, a neat liquid solution at room temperature that vitrifies as such upon flash freezing;
- $[^{13}\text{C}]$ -urea, a solid system at room temperature added with specific agents to promote glass formation once suddenly plunged in liquid helium.

$[1-^{13}\text{C}]$ -pyruvic acid has been investigated in great detail and for different experimental conditions by Ardenkjaer-Larsen and collaborators. In particular, the behaviour of the main parameters describing the DNP process have been determined for different trityl radical concentrations [41]. Results in terms of build up curves and polarization levels are recalled in FIG. 8, panel A. P_n^∞ reaches its maximum value ($P_n^\infty = 0.64$) when the electron concentration is 14.1 mM and therefore it significantly decreases on moving to 18.5 mM ($P_n^\infty = 0.58$) and 45.4 mM ($P_n^\infty = 0.23$). In parallel, a monotonic decrease of the polarization time T_{pol} from a maximum of 5000 s to a minimum of 475 s is observed. A similar trend was reported in [42] for a sample of $[^{13}\text{C}]$ -urea, actually one of the first endogenous molecules studied for biomedical applications, dissolved in glycerol to give a nearly saturated solution. On increasing the trityl concentration from 15 to 25 mM (FIG. 8, panel B), the build up curves speed up while the sample experiences a strong reduction of P_n^∞ (about a factor 2). Despite the different nature of the samples, a higher number of electrons is always associated to shorter T_{pol} and lower P_n^∞ .

As far as the influence of the addition of small amounts of Gd-complexes on the DNP behaviour is concerned, a broad systematic study has been reported by Lumata and collaborators [43]. They investigated the effect of Gd-HP-DO3A (ProHance, Bracco Imaging) on 1.4 M $[1-^{13}\text{C}]$ -sodium pyruvate samples in a 1:1 glycerol/water glassing matrix doped with three different radical types (trityl,

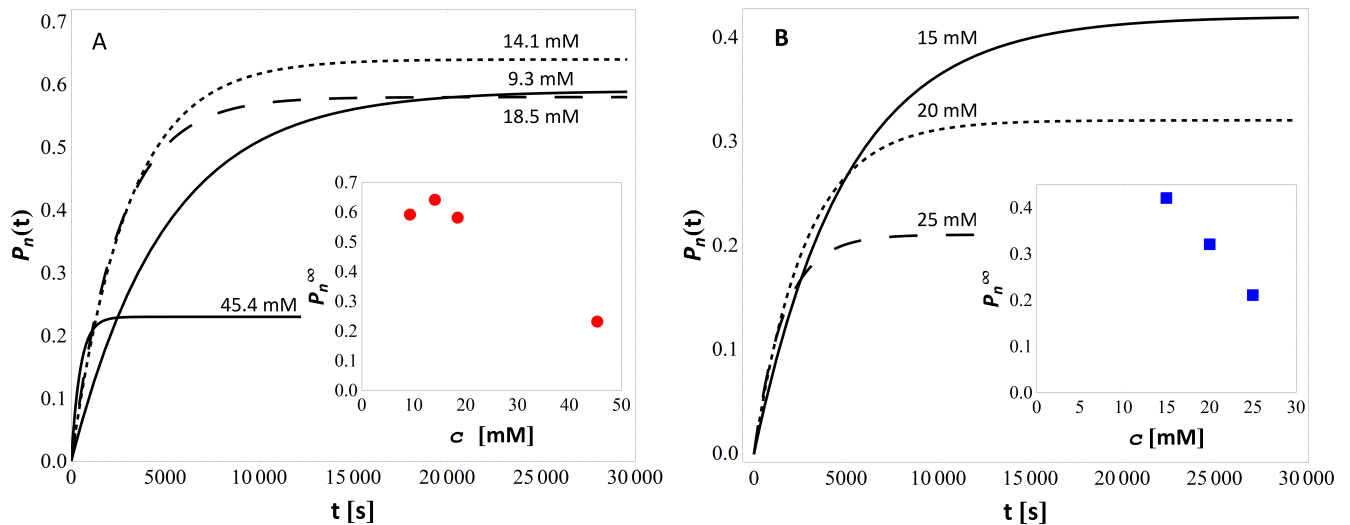


FIG. 8: A: Polarization build up curves and (inset) final polarization P_n^∞ versus electron concentration c , reproduced according to the experimental data reported in [41] acquired on [1-¹³C]-pyruvic acid samples at magnetic field $B_0 = 4.64$ T (corresponding to a microwave frequency of about 130 GHz), $T = 1.15$ K and trityl concentration ranging from 9.3 to 45.4 mM. B: Build up curves and (inset) final polarization of [¹³C]-urea in glycerol acquired at $B_0 = 3.35$ T (*i.e.* about 94 GHz electron resonance frequency) and $T = 1.2$ K with trityl concentration from 15 to 25 mM (data from [42]).

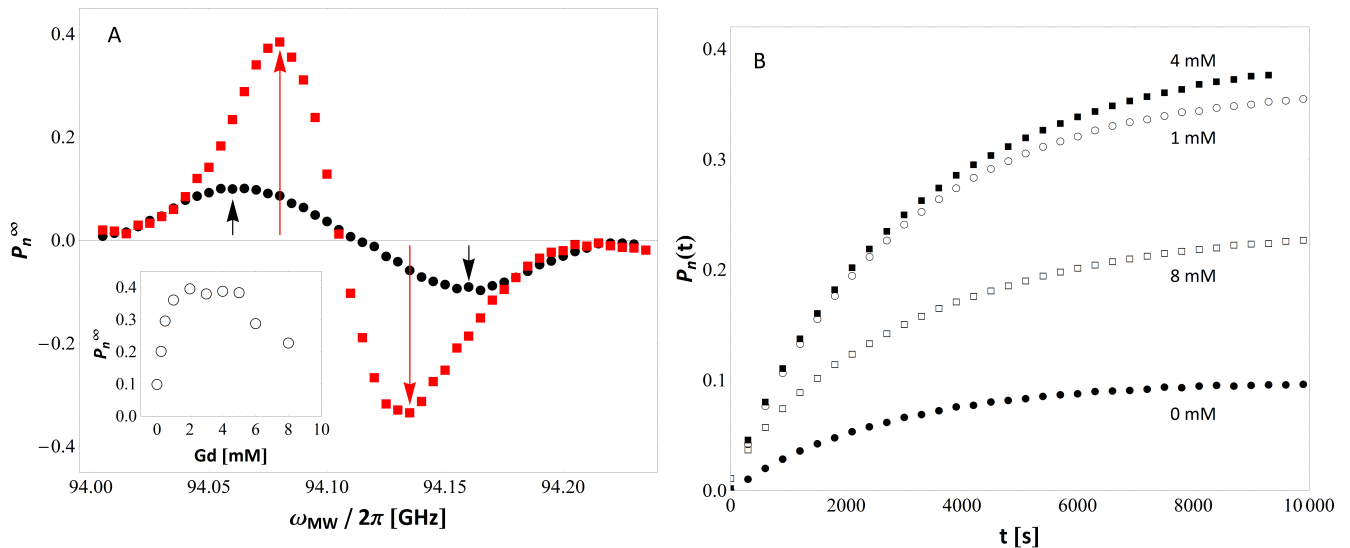


FIG. 9: Effect of gadolinium doping on [¹³C]-sodium pyruvate, data from [43]. A: Microwave spectrum for the undoped sample (black circles) and for the gadolinium-5 mM sample (red squares). The up and down arrows indicate the position of the positive and negative polarization peaks, respectively. In the inset the maximum positive polarization P_n^∞ as a function of gadolinium concentration is represented. B: Representative polarization build up curves for different concentrations of gadolinium. The time course of polarization looks not significantly affected by the gadolinium addition. Data were collected at 3.35 T and 1.4 K using a 100 mW microwave source operating at about 94 GHz.

nitroxide, BDPA). In FIG. 9 the data obtained for the solution containing 15 mM of trityl radical and different gadolinium amounts (0-8 mM) are summarized. A comparison between the microwave spectra with and without gadolinium is shown in panel A. The addition of gadolin-

ium leads to two main outcomes, a reduced separation between the positive and the negative polarization peaks and a nearly linear increase of P_n^∞ as the concentration of the rare earth [Gd] goes from 0 to 2 mM. By further increasing [Gd], the steady state polarization first

reaches a plateau and then declines for $[Gd] > 5$ mM. The maximum P_n^∞ achieved upon gadolinium doping is approx. 4 times higher than what obtained in the undoped sample. Polarization times, on the other hand, were found to be only slightly affected by the gadolinium doping (FIG. 9, panel B). Similar results hold for BDPA radicals, whereas much less pronounced effects were observed when nitroxides are used for polarizing the sample. It is worth to notice that both carbon and hydrogen nuclei are involved in TM-DNP of samples prepared with nitroxides; this introduces a further degree of freedom in the problem, pushing it outside the field of validity of the theoretical model presented in the Section III.

Appendix B: Rate equation system

In order to simulate the time evolution of the electron polarization profile, the same approach proposed in [12, 13] has been used. The ESR line was modeled by a Gaussian function truncated at 3σ , with $\sigma = 27$ MHz to reproduce the behaviour of trityl based DNP samples [10], and split into $N_p = 45$ electron packets of width $\delta\omega \approx 3.5$ MHz, characterized by a polarization $P_{e,i}(t)$ (indicated here with $P_{e,i}$), with $i = 1, N_p$. We have checked that our results don't change on increasing the number of packets and thus can be considered as a good reproduction of the continuum limit. The MW irradiation was assumed to be strong enough to saturate a given packet i_0 , voiding its polarization. Then, under the assumption of weak coupling between the electron and nuclear spin systems (see the third assumption at Section III), the

time evolution of the remaining packets can be derived using the same rate equation approach developed in [12]. In particular the three processes sketched in FIG. 2 lead to the following system of rate equations:

$$\begin{aligned} \frac{dP_{e,i}}{dt} = & \frac{P_0 - P_{e,i}}{T_{1e}} + \frac{1}{4T_{\text{CSD}}} \left(f_{i-1}f_i f_{i+1} \Pi_{e,i} \right. \\ & \left. - \frac{1}{2} f_{i+2} f_{i+1}^2 \Pi_{e,i+1} - \frac{1}{2} f_{i-2} f_{i-1}^2 \Pi_{e,i-1} \right) \quad (\text{B1}) \\ & + \frac{f_{i-1}(P_{e,i-1} - P_{e,i}) + f_{i+1}(P_{e,i+1} - P_{e,i})}{T_{\text{DSD}}} \end{aligned}$$

where $P_0 = \tanh[\beta_L \omega_e]$ ($\omega_e = \gamma_e B_0$, with $\gamma_e = 2\pi \cdot 28.025$ GHz/T) and $\Pi_{e,i}$ is given by the expression:

$$\Pi_{e,i} = (P_{e,i-1} + P_{e,i+1}) (1 + P_{e,i}^2) - 2(1 + P_{e,i-1} P_{e,i+1}) P_{e,i}$$

The system (B1) has been numerically solved to compute $P_{e,i}$ imposing a discrete time step dt , so that:

$$\frac{1}{dt} = \frac{1}{T_{1e}} + \frac{\sum_i f_i^2 f_{i-1} f_{i+1}}{2T_{\text{CSD}}} + \frac{\sum_i f_i f_{i+1}}{T_{\text{DSD}}}.$$

The function $P_e(\omega, t)$ to be used in Eq.(3) was thus obtained by imposing $\omega = \omega_0 + 2\pi (i - \frac{N_p+1}{2}) \delta\omega$ and $\omega_n = 2\pi \cdot 9 \delta\omega \approx 2\pi \cdot 35$ MHz which corresponds to the ^{13}C Larmor frequency at $B_0 = 3.35$ T. Finally, the steady state polarization $P_e^\infty(\omega)$ for Eq. 2 has been calculated as the limit of $P_e(\omega, t)$, for $t \rightarrow \infty$.

-
- [1] P. Dutta, G. V. Martinez and R. J. Gillies Biophys Rev DOI 10.1007/s12551-012-0099-2 (2012).
- [2] J. Kurhanewicz, D. B. Vigneron, K. Brindle, E. Y. Chekmenev, A. Comment, C. H. Cunningham, R. J. DeBerardinis, G. G. Green, M. O. Leach, S. S. Rajan, R. R. Rizi, B. D. Ross, W. S. Warren and C. R. Malloy, Neoplasia **13**, 81 (2011).
- [3] J. H. Ardenkjaer-Larsen, B. Fridlund, A. Gram, G. Hansson, L. Hansson, M. H. Lerche, R. Servin, M. Thanning and K. Golman, Proc. Natl. Acad. Sci. **100**, 10158 (2003).
- [4] A. Abragam and M. Goldman, Nuclear magnetism: order and disorder. Oxford: Clarendon Press, (1982).
- [5] Y. Hovav, A. Feintuch and S. Vega, J. Chem. Phys. **134**, 074509 (2011).
- [6] Y. Hovav, A. Feintuch and S. Vega, J. Magn. Reson. **207**, 176 (2010).
- [7] A. Karabanov, A. van der Drift, L. J. Edwards, I. Kuprov and W. Köckenberger, Phys. Chem. Chem. Phys. **14**, 2658 (2012).
- [8] Y. Hovav, A. Feintuch and S. Vega, J. Magn. Reson. **214**, 29 (2012).
- [9] D. Shimon, Y. Hovav, A. Feintuch, D. Goldfarb and S. Vega, Phys. Chem. Chem. Phys. **14**, 5729 (2012).
- [10] J.H. Ardenkjaer-Larsen, S. Macholl and H. Johannesson, App. Magn. Reson. **34**, 509 (2008).
- [11] S. Jannin, A. Comment and J. J. van der Klink, Appl. Mag. Res. **43**, 59 (2012).
- [12] S. Colombo Serra, A. Rosso and F. Tedoldi, Phys. Chem. Chem. Phys. **14**, 13299 (2012).
- [13] S. Colombo Serra, A. Rosso and F. Tedoldi, Phys. Chem. Chem. Phys. **15**, 8416 (2013).
- [14] M. Thanning, R. Servin, International Patent Publication Number WO 2007/064226 A2, W. I. P., Norway.
- [15] F. A. Gallagher, M. I. Kettunen, S. E. Day, D. E. Hu, J. H. Ardenkjaer-Larsen, R. int Zandt, P. R. Jensen, M. Karlsson, K. Golman, M. H. Lerche et al., Nature **453**, 940 (2008).
- [16] S. E. Bohndiek, M. I. Kettunen, D. E. Hu, B. W. C. Kennedy, J. Boren, F. A. Gallagher, K. M. Brindle, J. Am. Chem. Soc. **133**, 11795 (2011).
- [17] M. A. Schroeder, H. J. Atherton, D. R. Ball, M. A. Cole, L. C. Heather, J. L. Griffin, K. Clarke, G. K. Radda, D. J. Tyler FASEB J., **23**, 2529 (2009).
- [18] S. E. Bohndiek, M. I. Kettunen, D. E. Hu, T. H. Witney, B. W. C. Kennedy, F. A. Gallagher, K. M. Brindle, Mol. Cancer Ther. **9**, 3278 (2010).
- [19] D. M. Wilson, K. R. Keshari, P. E. Z. Larson, A. P. Chen, S. Hu, M. Van Criekinge, R. Bok, S. J. Nelson, J.

- M. Macdonald, D. B. Vigneron, et al. *J. Magn. Reson.* **205**, 141 (2010).
- [20] F. A. Gallagher, M. I. Kettunen, D. E. Hu, P. R. Jensen, R. int Zandt, M. Karlsson, A. Gisselsson, S. K. Nelson, T. H. Witney, S. E. Bohndiek, et al. *Proc. Natl. Acad. Sci. U.S.A.* **106**, 19801 (2009).
- [21] P. R. Jensen, T. Peitersen, M. Karlsson, R. int Zandt, A. Gisselsson, G. Hansson, S. Meier, M. H. Lerche, *J. Biol. Chem.* **284**, 36077 (2009).
- [22] R. E. Hurd, Y.F. Yen, J. Tropp, A. Pfefferbaum, D. M. Spielman, D. Mayer, *J. Cereb. Blood Flow Metab.* **30**, 1734 (2010).
- [23] M. Karlsson, P. R. Jensen, R. int Zandt, A. Gisselsson, G. Hansson, J. O. Duus, S. Meier, M. H. Lerche, *Intl. J. Cancer* **127**, 729 (2010).
- [24] A. Z. Lau, A. P. Chen,; N. R. Ghugre, V. Ramanan, W. Lam, K. A. Connelly, G. A. Wright, C. H. Cunningham, *Magn. Reson. Med.* **64**, 1323 (2010).
- [25] T. H. Witney, M. I. Kettunen, D. E. Hu, F. A. Gallagher, S. E. Bohndiek, R. Napolitano, K. M. Brindle, *Br. J. Cancer* **103**, 1400 (2010).
- [26] S. E. Day, M. I. Kettunen, M. K. Cherukuri, J. B. Mitchell, M. J. Lizak, H. D. Morris, S. Matsumoto, A. P. Koretsky, K. M. Brindle, *Magn. Reson. Med.* **65** 557 (2011).
- [27] F. A. Gallagher, M. I. Kettunen, S. E. Day, D. E. Hu, M. Karlsson, A. Gisselsson, M. H. Lerche, K. M. Brindle, *Magn. Reson. Med.* **66**, 18 (2011).
- [28] S. Hu, A. Balakrishnan, R. A. Bok, B. Anderton, P. E. Z. Larson, S. J. Nelson, J. Kurhanewicz, D. B. Vigneron, A. Goga, *Cell Metab.* **14**, 131 (2011).
- [29] J. D. MacKenzie, Y. F. Yen, D. Mayer, J. S. Tropp, R. E. Hurd, D. M. Spielman, *Radiology* **259**, 414 (2011).
- [30] M. H. Lerche, S. Meier, P. R. Jensen, H. Baumann, B. O. Petersen, M. Karlsson, J. O. Duus, J. H. Ardenkjaer-Larsen, *J. Magn. Reson.* **203**, 52 (2010).
- [31] P. R. Jensen, M. Karlsson, S. Meier, J. O. Duus, M. H. Lerche, *Chem. Eur. J.* **15**, 10010 (2009).
- [32] A. K. Grant, E. Vinogradov, X. Wang, R. E. Lenkinski, D. C. Alsop, *Magn. Reson. Med.* **66**, 746 (2011).
- [33] S. Macholl, H. Johannesson and J.H. Ardenkjaer-Larsen, *Phys. Chem. Chem. Phys.* **12**, 5804 (2010).
- [34] A. Comment, B. van den Brandt, K. Uffman, F. Kurdzsau, S. Jannin, J.A. Konter, P. Hautle, W.TH. Wenckebach, R. Gruetter and J.J. van der Klink, *Magn. Res. Part B* **31B**, 255 (2007).
- [35] M. Borghini, *Phys. Rev. Lett.* **20**, 419 (1968).
- [36] B. N. Provotorov, *Soviet Phys. J. Exp. Theor. Phys.* **14**, 1126 (1962).
- [37] B. N. Provotorov, *Phys. Rev.* **128**, 75 (1962).
- [38] B. N. Provotorov, *Soviet Phys. J. Exp. Theor. Phys.* **15**, 611 (1963).
- [39] B. N. Provotorov, *Soviet Phys. Solid State* **4**, 2155 (1963).
- [40] C. T. Farrar, D. A. Hall, G. J. Gerfen, S. J. Inati, and R. G. Griffin, *J. Chem. Phys.* **114**, 4922 (2001).
- [41] H. Johannesson, S. Macholl and J. H. Ardenkjaer-Larsen, *J. Magn. Reson.* **197**, 167 (2009).
- [42] J. Wolber, F. Ellner, B. Fridlund, A. Gram, H. Johannesson, G. Hansson, L. H. Hansson, M. H. Lerche, S. Mansson, R. Servin, M. Thaning, K. Golman and J.H. Ardenkaer-Larsen, *Nuclear Instruments and Methods in Physics Research A* **526**, 173 (2004).
- [43] L. Lumata, M. Merritt, C. Malloy, A. D. Sherry and Z. Kovacs, *J. Phys. Chem. A* **116**, 5129 (2012).
- [44] Conversely to what we did in the past [12, 13], we chose here to use a different symbol for the typical time of this four electron mechanism previously named T_{2e} . This in order to better distinguish the microscopic events (T_{CSD}) partially responsible for the energy exchange between different electron spins from the collective time (usually reported as T_{2e}) that describes the spin-spin relaxation from a thermodynamic point of view.